PROCEEDINGS OF SCIENCE

ONLINE ICRC 2021
THE ASTROPARTICLE PHYSICS CONFERENCE
Berlin | Germany
37th International Cosmic Ray Conference
12–23 July 2021

Stereoscopic and monoscopic operation of the five IACTs in the TAIGA experiment

A.A.Grinyuk,[a,b,*] **E.B.Postnikov**[b,*] **and P.A.Volchugov**[b,c,*] **on behalf of the TAIGA Collaboration**
(a complete list of authors can be found at the end of the proceedings)

[a]Joint Institute for Nuclear Research, Joliot-Curie 6, Dubna, Moscow Region, 141980, Russia
[b]Lomonosov Moscow State University Skobeltsyn Institute of Nuclear Physics (MSU SINP), Leninskie gory 1(2), GSP-1, Moscow, 119991, Russia
[c]Institute of Applied Physics, Irkutsk State University (API ISU), Gagarin Blvd. 20, Irkutsk, 664003, Russia
E-mail: andrei.grinyuk@gmail.com, evgeny.post@gmail.com, pvol4@yandex.ru

The 2nd TAIGA imaging air Cherenkov telescope (IACT) has successfully been put into operation in the Tunka Valley in fall 2020. Currently three more telescopes are under construction and completion. The ability to use the telescopes in the so-called stereo mode of image analysis by taking into account the unusually large distance between them (from 320 m to 500 m), well exceeding the inter-telescope distances in conventional IACT stereo systems, is being explored and discussed. The results of the dedicated Monte Carlo are compared with the experiment data from the 1st and the 2nd TAIGA-IACT.

37th International Cosmic Ray Conference (ICRC 2021)
July 12th – 23rd, 2021
Online – Berlin, Germany

*Presenter

PoS(ICRC2021)713

1. Introduction

The TAIGA experiment, where TAIGA stands for Tunka Advanced Instrument for cosmic ray physics and Gamma-ray Astronomy, combines detection of both ultra-high-energy cosmic rays (>100 TeV) and very-high-energy gamma rays (>10 TeV) at the same Tunka Astrophysical Center in the Tunka Valley near Lake Baikal [1, 2]. The northernmost location of TAIGA allows long observation times on the sources with large declinations.

For gamma-ray detection, TAIGA uses imaging air Cherenkov telescopes (IACTs) and wide-angle timing stations named TAIGA-HiSCORE (High Sensitivity Cosmic ORigin Explorer). The information from the stations (arrival direction and core position) will be used by an IACT even if no other IACT detects the same event. However, some portion of events will be detected by multiple telescopes and analyzed with a technique known as stereoscopy.

Currently two imaging air Cherenkov telescopes are operating, and the 3rd one has already been installed but with neither mirrors nor camera due to COVID-19 work restrictions. Its deployment is planned in fall 2021; the 4th and 5th IACT will be installed in 2 years. The distance between the IACTs will be at least 250 m – that is the distance between the central IACT of the group (IACT#4) and peripheral ones.

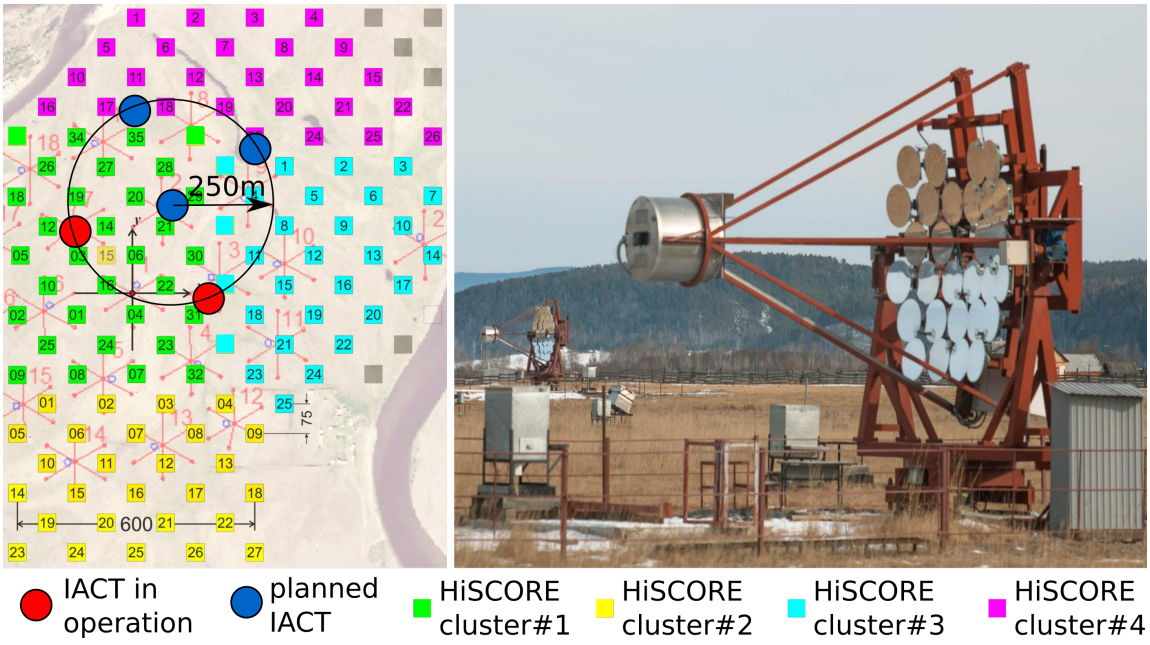

Figure 1: Location of the HiSCORE stations along with IACTs in the Tunka Valley

2. TAIGA-IACTs

Optical design of the IACTs is of Davies-Cotton type with 34 spherical mirror tiles, each with a 60-cm diameter (9.6 m^2 total area), and a focal length of 4.75 m. The imaging camera for the 1st IACT comprises 560 photomultipliers (PMTs) with a 19-mm diameter; for the 2nd IACT it consists of 595 PMTs. The FoV of the camera is 9.6^o (0.36^o per pixel) with a point spread function of 0.07^o [2].

The first test sources selected for observation were the Crab Nebula and Mrk 421. Both these sources were successfully detected [3, 4] in the preliminary data analysis of stand-alone operation of the 1st IACT.

3. Monte-Carlo simulation and comparison with experimental data

Simulation of extensive air showers (EAS) was carried out in CORSIKA [5] version 7.35 with QGSJET-II-04 [6] model for high-energy interactions and GHEISHA-2002d [7] for low-energy interactions. Positions of five TAIGA-IACTs were used in input files. Showers from primary protons and gamma rays were simulated. Energy range was 5–100 TeV for protons and 2–50 TeV for gamma rays, both distributed according to exponential spectrum with the index -2.6. Zenith angles 30°–40° correspond to the Crab Nebula observation in the Tunka Valley. Photon bunches from CORSIKA output were ray-traced in a dedicated C++ optical simulation program [8]. This program models optical properties of IACT all the way to PMT photocathodes and outputs individual photoelectrons at the IACT camera.

Photoelectron data are input for the detector response simulation, which includes triggering and analog readout procedures [8]. Trigger decision is at exceeding of the set threshold (10 p.e.) by the signal in two adjacent PMTs in one cluster of 28 PMTs within the set time window.

After passing the hardware trigger, the events can be analyzed in several stereo modes, such as 2 +, 3 +, 4 + and 5. For example, the 2+ mode means that the analysis involves events that triggered 2 or more telescopes.

To verify the equivalence of simulation and experimental data, distributions of the image *size* for the events detected by the both telescopes were constructed based on real data and Monte Carlo (Fig.2a). *Size* is the total number of photoelectrons (p.e.) in the image [9]. The counting rate of events detected by the both telescopes is ∼10 times lower than that of single events both in the simulated samples and in the experiment.

4. Effective area

To estimate the effective area, MC simulation of a setup with 5 telescopes was used. Showers were scattered over area of $\sim$ 3 km^2 around the central telescope (TAIGA-IACT04). A total of $4 \cdot 10^5$ events were generated for MC data bank. Based on these data, for each 5 TeV bin, the number gamma-initiated events was calculated. At the same time, the number of events in the same bins that passed the trigger was calculated. Note that from the events that passed the trigger, events containing boundary pixels of camera were excluded, since the analysis of such events is a more complex task. The ratio of the number of generated particles to the number of particles passed through the trigger multiplied by the area of scattering of gamma rays gives the effective area of the installation in a given energy range.

We present the effective installation area for different types of analyzed events. It was obtained that for 2+ events at 10 TeV, the effective area is 0.45 km^2 and reaches a maximum of 0.9 km^2 at an energy of 22 TeV. Above this energy, the registration efficiency does not increase, since the events become more extended and are rejected by the cut at the boundary pixels of camera.

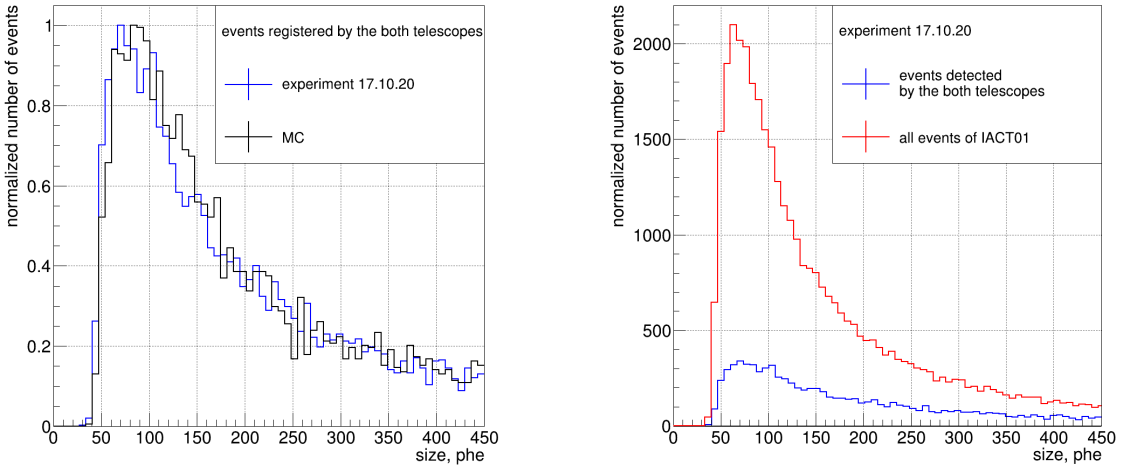

(a) **(b)**

Figure 2: Comparison of: a) experimental and MC distribution of *size* of events detected by the both telescopes of the TAIGA-IACT; b)experimental distribution of size of all events TAIGA-IACT01 and events detected by the both telescopes

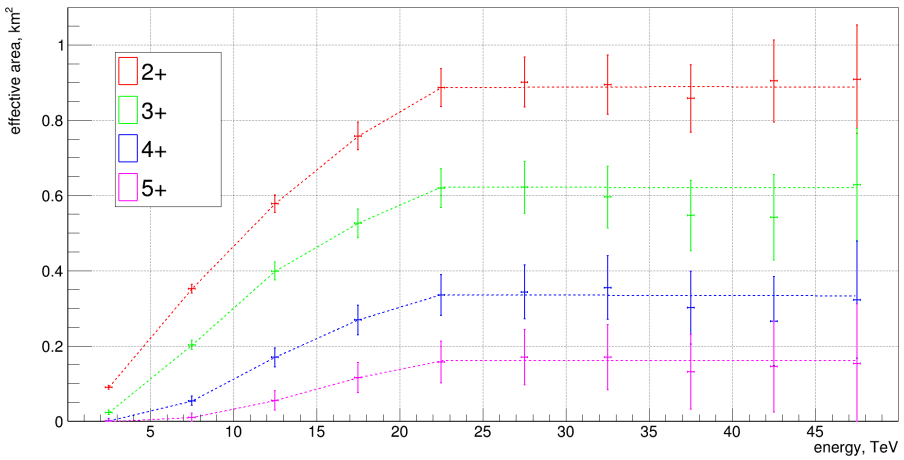

Figure 3: Effective area of the TAIGA-IACT installation

5. Hadron suppression and sensitivity

Since the detection efficiency at low energies (a few TeV) is rather low, the analysis included gamma rays and hadrons with energies above 10 TeV. The analysis involves applying cuts to sets of modeled particles. In this chapter we consistently show how selected cuts influence on the selection of events.

Basic suppression

First of all, it is necessary to take into account the suppression by the telescope hardware trigger. For gamma rays above 10 TeV, 97% of the generated events pass the trigger, whereas the

fraction of hadrons after the hardware trigger is 51% due to the fact that the arrival directions of gamma rays are concentrated in a narrow region in the center of the camera FoV (within 0.1°) and those of hadrons are uniformly distributed over the entire camera (within 5°) leading to the loss of the fraction of events outside the camera FoV.

After the trigger of the telescope, all events are divided into several parts, in accordance with number of triggered telescopes(2+, 3+ etc.). The further description of the hadron suppression procedure includes events of 2+ type. The selection of events detected in this way leads to the conservation of 76% of gamma rays and 23% of hadrons from the MC data bank.

The next step is to apply a cut to the boundary pixels of camera. It leads to suppression coefficients of 0.73 and 0.18 for gamma rays and hadrons, respectively.

Application of a cut $size > 100$ p.e. results in suppression coefficients of 0.6 for gamma and 0.14 for hadrons. Cut on the image $size$ is necessary to improve the accuracy of determining the image orientation.

All the cuts described in this section, such as a hardware trigger, choice of the type of triggered events (2+, 3+ etc.), exclusion of boundary camera pixels and $size > 100$ p.e., are hereafter referred to as basic suppression.

Determination of source location

When observing the known point sources of gamma rays, the direction of arrival of gamma rays in the FoV of the telescope is known, which is incorrect for hadrons. Hence, reconstruction of the source position can be useful for gamma-hadron separation.

To solve this problem, the arrival direction of particles was determined as the weighted average position of the intersection points of the major axes of all ellipses. The image axes in the two triggered telescopes will intersect at the point:

$$x = \frac{b_2 - b_1}{a_1 - a_2} \text{ and } y = a_1 x + b_1$$

Each pair of telescopes gives a point, which is filled into a histogram with a weight of

$$\frac{size_1 + size_2}{\sum_i^{N_{trig}} size_i} \cdot sin\theta,$$

where θ is the angle between intersecting lines [10], N_{trig} - number of triggered telescopes.

The resulting direction of arrival of the event is determined as the average of the histogram filled with the intersection points:

$$x_{mean} = \frac{1}{N_{bin}} \sum_i^{N_{bin}} \sum_j^{N_{bin}} y_{ji} \text{ and } y_{mean} = \frac{1}{N_{bin}} \sum_j^{N_{bin}} \sum_i^{N_{bin}} x_{ij},$$

where N_{bin} is the number of histogram bins along the axis (equal for x and y).

We present the errors of determining arrival direction of events in the telescope's FoV (Fig. 4). Cut on this value was defined as a circle with containment radii 68% of the events that passed the basic suppression. Further, this parameter is called r_{68}. The angular resolution for the 2+ events type is $r_{68} = 0.2\ ^\circ$ and gives suppression relative to the MC data bank of 0.4 for gamma > 10 TeV and $5 \cdot 10^{-4}$ for hadrons > 10 TeV.

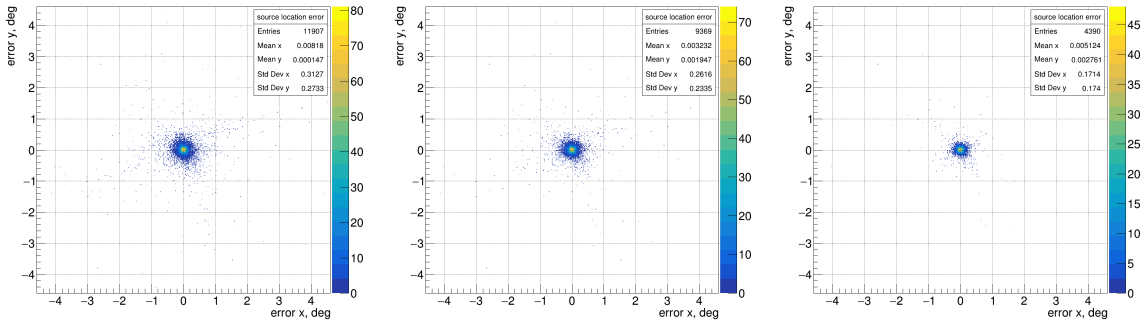

(a) 2+(stereo) **(b)** 3+ **(c)** 4+

Figure 4: Error of determining source location in telescope FoV for different event types.

Another approach to determining the position of the source in the FoV of the telescope was applied. It is based on minimizing the following functional:

$$f = \left(\sum_{i}^{N_{trig}} \frac{\Delta\theta_i^2}{\sigma_i^2} \right) + \frac{\Delta\Omega^2}{\sigma_\Omega^2}$$

where $\Delta\theta_i^2$ is the angles between the major axes of the ellipses and the lines connecting the center of gravity (COG) of the image with the assumed position of the source, $\Delta\Omega^2$ is the distance (angle) between the assumed position of the source and the true one. The σ_i depends on the "width" and "length" parameters and was defined in [10]. σ_Ω depends on the *size* and is determined so that the average value of $\frac{\Delta\theta_i^2}{\sigma_i^2}$ is as close as possible to $\frac{\Delta\Omega^2}{\sigma_\Omega^2}$ in minimization. This functional selects the position of the source near the intersection of the major axes of the ellipses and at a small distance from the true arrival direction of events. The cut $f < 10$ gives suppression of 0.38 and $4{\cdot}10^{-4}$ for gamma rays and hadrons, respectively.

Normalized width

In the stereoscopic approach, the normalized width is analogous to the "width" parameter[9] - RMS along the minor axis of the ellipse. It is defined as follows[11]:

$$w = \frac{1}{N_{tel}} \left[\sum_{i}^{N_{trig}} \frac{width_i - w_m(r_i, size_i)}{w_{MAD}(r_i, size_i)} \right]$$

Where N_{tel} is the number of triggered telescopes, $width_i$ is the *width* in a given triggered telescope, $w_m(r_i, size_i)$ is the median value of the width characteristic of events with a given size($size_i$) and distance to the shower axis(r_i). $w_{MAD}(r_i, size_i)$ - median absolute deviation, distribution of *width* typical for a given distance to the EAS axis(r_i) and a given event size($size_i$).

w_{MAD} and w_m are template values predefined from the simulation. To determine these values, we need to reconstruct the core position. This was done in several ways:

- by weighted averaging of intersection points of the major axes of the ellipses, similar to determining the position of the source in the telescope's FoV, but in this case the ellipses are

>10TeV	MC generated	hardware trigger	2+ events	exclusion of edge pixels	size > 100 p.e.	number of events within $r_{68} = 0.2°$	f<10	w<0
gamma	19627	19128	14973	14389	11907	8116	7454	3587
hadrons	215765	110354	48784	39550	29384	113	92	4

Table 1: Summary table of cuts influence

located in the ground frame, where the telescopes are located relative to each other (in the case of determining the position of the source in the telescope FoV, the ellipses were located in a nominal frame, the joint FoV of the telescopes);

- using the procedure for minimizing the distances to the major axes of the ellipses [11].

Each of these approaches can be applied to the reconstruction based on: a) the major axes of the ellipses, b) the distance parameter [9] - the distance between the COG of the image and the known position of the source.

The use of the later method improves the accuracy of determining core position. So, for 4+ events, RMS = 16 m and grows with a decrease in the number of triggered telescopes up to ~ 60 m for 2+ events. To determine ω_m and ω_{MAD} for each interval of distances to the shower core, with a step of 100 m, the dependence of these parameters on the size was obtained. As a result, the distribution of the parameter "normalized width" was obtained for the simulated events. Using the cut $\omega < 0$ gave suppression of 0.2 for gamma rays and $2 \cdot 10^{-5}$ for hadrons. Summary table describing the effect of cuts on simulated event samples is presented in Tab.1.

On the basis of the obtained coefficients of suppression of hadrons and gamma rays, the integral sensitivity of the TAIGA-IACT installation was calculated. The initial number of hadrons was estimated based on the approximation of the CR spectrum of the DAMPE observatory [12, 13]. As a result, for gamma rays with energies >10 TeV, we expect the sensitivity for 100 hours of observation $\sim 1.5 \cdot 10^{-12}$ TeV^{-1}cm^{-2}s^{-1}.

Conclusion

A sufficiently large effective area (~1 km^2) and good angular resolution (r_{68}~ 0.2°) for gamma rays with energy above 10 TeV was derived from Monte Carlo simulation of 5 IACTs in TAIGA. Both the sensitivity ($\sim 1.5 \cdot 10^{-12}$ TeV^{-1}cm^{-2}s^{-1} for 100 h of observation) and northernmost location (51.49°N, 103.04°E) allow a detailed measurement of the energy spectra (>10 TeV) of many sources from the Crab Nebula and Mrk 501 to Dragonfly Nebula, Boomerang, ARGO J2031+4157 etc. and probably SNR CTA 1 and Tycho.

Since fall 2021 three IACTs will be operating and available for the stereoscopic analysis. Two more IACTs are to be deployed by 2023.

Acknowledgments

The work was performed at the UNU "Astrophysical Complex of MSU-ISU" (agreement 13.UNU.21.0007) and is supported by the Russian Foundation for Basic Research (grants #19-52-

44002, 19-32-60003), Russian Science Foundation (grant #19-72-20067 (Sections 4, 5)), Russian Federation Ministry of Science and High Education (projects FZZE-2020-0017, FZZE-2020-0024).

References

[1] N. Budnev et al., *TAIGA—An Innovative Hybrid Array for High Energy Gamma Astronomy, Cosmic Ray Physics and Astroparticle Physics*, *Physics of Atomic Nuclei* **84** (2021) 362.

[2] L. Kuzmichev et al., *Cherenkov EAS arrays in the Tunka astrophysical center: From Tunka-133 to the TAIGA gamma and cosmic ray hybrid detector*, *Nucl. Instrum. Methods Phys Res., Sect. A* **952** 161830.

[3] E. Postnikov et al., *First detection of gamma-ray sources at TeV energies with the first imaging air cherenkov telescope of the TAIGA installation*, *Journal of Physics: Conference Series* **1690** (2020) 012023.

[4] L. Sveshnikova et al., *Detecting Gamma Rays with Energies Greater than 3–4 eV from the Crab Nebula and Blazar Markarian 421 by Imaging Atmospheric Cherenkov Telescopes in the TAIGA Experiment*, *Bull. Russ. Acad. Sci. Phys.* **85** (2021) 398–401.

[5] D. Heck et al., *CORSIKA: a Monte Carlo code to simulate extensive air showers*, Technical Report FZKA-6019, Forschungszentrum Karlsruhe (1998).

[6] S. Ostapchenko, *Monte Carlo treatment of hadronic interactions in enhanced Pomeron scheme: QGSJET-II model*, *Phys. Rev. D* **83** (2011) 014018 [1010.1869].

[7] H. Fesefeldt, *The simulation of hadronic showers: physics and applications*, Tech. Rep. Physikalisches Institut, Technische Hochschule Aachen (PITHA) (1985).

[8] E. Grinyuk, N. Postnikov and L. Sveshnikova, *Monte Carlo Simulation of the TAIGA Hybrid Gamma-Ray Experiment*, *Physics of Atomic Nuclei* **83** (2020) 262.

[9] A.M. Hillas, *Cerenkov Light Images of EAS Produced by Primary Gamma Rays and by Nuclei*, in *19th International Cosmic Ray Conference (ICRC19)*, vol. 3, p. 445, 1985.

[10] W. Hofmann et al., *Comparison of techniques to reconstruct vhe gamma-ray showers from multiple stereoscopic Cherenkov images*, *Astropart. Phys.* **122** (1999) 135.

[11] H. Krawczynski et al., *Gamma-Hadron Separation Methods for the VERITAS Array of Four Imaging Atmospheric Cherenkov Telescopes*, *Astropart. Phys.* **25** (2006) 380.

[12] DAMPE collaboration, *Measurement of the cosmic-ray proton spectrum from 40 GeV to 100 TeV with the DAMPE satellite*, *Sci. Adv.* **5** (2019) [1909.12860].

[13] F. Alemanno et al., *Measurement of the cosmic ray helium energy spectrum from 70 GeV to 80 TeV with the DAMPE space mission*, 2105.09073.

Full Authors List: TAIGA Collaboration

I. I. Astapov[2] A. K. Awad[10] P. A. Bezyazeekov[3] M. Blank[10] A. N. Borodin[4] A. V. Bulan[1] M. Brueckner[5] N. M. Budnev[3] A. Chiavassa[6] A. N. Dyachok[3] A. R. Gafarov[3] A. Yu. Garmash[7,8] V. M. Grebenyuk[4,9] O. A. Gress[3] T. I. Gress[3] O. G. Grishin[3] A. A. Grinyuk[4] D. Horns[10] N. N. Kalmykov[1] V. V. Kindin[2] S. N. Kiryuhin[3] R. P. Kokoulin[2] K. G. Kompaniets[2] E. E. Korosteleva[1] V. A. Kozhin[1] E. A. Kravchenko[7,8] A. P. Kryukov[1] L. A. Kuzmichev[1] A. A. Lagutin[11] M. Lavrova[4] B. K. Lubsandorzhiev[12] N. B. Lubsandorzhiev[1] A. D. Lukanov[12] D. S. Lukyantsev[3] R. R. Mirgazov[3] R. Mirzoyan[13,3] R. D. Monkhoev[3] E. A. Osipova[1] A. L. Pakhorukov[3] A. Pan[4] M. I. Panasyuk[1] L. V. Pankov[3] A. A. Petrukhin[2] V. A. Poleschuk[3] M. Popesku[14] E. G. Popova[1] A. Porelli[5] E. B. Postnikov[1] V. V. Prosin[1] V. S. Ptuskin[15] A. A. Pushnin[3] R. I. Raikin[11] A. Y. Razumov[1] G. I. Rubtsov[12] E. V. Ryabov[3] Y. I. Sagan[4,9] V. S. Samoliga[3] Yu. A. Semeney[3] A. A. Silaev[1] A. A. Silaev(junior)[1] A. Yu. Sidorenkov[12] A. V. Skurikhin[1] M. Slunecka[4] A. V. Sokolov[7,8] C. Spiering[5] L. G. Sveshnikova[1] V. A. Tabolenko[3] B. A. Tarashansky[3] L. G. Tkachev[4,9] R. Togoo[16] M. Tluczykont[10] N. Ushakov[12] A. Vaidyanathan[7] P. A. Volchugov[1] N. V. Volkov[11] D. Voronin[12] R. Wischnewski[5] A. V. Zagorodnikov[3] D. P. Zhurov[3,17] I. I. Yashin[2]
[1]Skobeltsyn Institute of Nuclear Physics, Moscow State University, Moscow, 119991 Russia [2]National Research Nuclear University MEPhI, Moscow, 115409 Russia [3]Research Institute of Applied Physics, Irkutsk State University, Irkutsk, 664003 Russia [4]Joint Institute for Nuclear Research, Dubna, Moscow oblast, 141980 Russia [5]Deutsches Elektronen-Synchrotron DESY, Zeuthen, 15738 Germany [6]Physics Department of the University of Torino and Istituto Nazionale di Fisica Nucleare, Torino, 10125 Italy [7]Novosibirsk State University, Novosibirsk, 630090 Russia [8]Budker Institute of Nuclear Physics, Siberian Branch, Russian Academy of Sciences, Novosibirsk, 630090 Russia [9]Dubna University, Dubna, Moscow oblast, 141980 Russia [10]Institut für Experimentalphysik, Universität Hamburg, Hamburg, D-22 761 Germany [11]Altai State University, Barnaul, Altai krai, 656049 Russia [12]Institute for Nuclear Research, Russian Academy of Sciences, Moscow, 117312 Russia [13]Max Planck Institute for Physics, Munich, 80805 Germany [14]Space Science Institute, Magurele, 077125 Romania [15]Pushkov Institute of Terrestrial Magnetism, Ionosphere and Radio Wave Propagation, Russian Academy of Sciences, Troitsk, Moscow, 142190 Russia [16]Institute of Physics and Technology Mongolian Academy of Sciences, Ulaanbaatar, Mongolia [17]Irkutsk National Research Technical University, Irkutsk, Russia

PoS(ICRC2021)713